RESEARCH ARTICLE

Effective buoyancy and CAPE: Some implications for tropical cyclones

R. K. Smith[1] | M. T. Montgomery[2]

[1]Meteorological Institute, Ludwig-Maximilians University, Munich, Germany

[2]Department of Meteorology, Naval Postgraduate School, Monterey, California

Correspondence
R. K. Smith, Meteorological Institute, Ludwig-Maximilians University, Munich, Germany.
Email: roger.smith@lmu.de

Abstract

We review the widely used concepts of "buoyancy" and "convective available potential energy" (CAPE) in relation to deep convection in tropical cyclones and discuss their limitations. A fact easily forgotten in applying these concepts is that the buoyancy force of an air parcel, as often defined, is non-unique because it depends on the arbitrary definition of a reference density field. However, when calculating CAPE, the buoyancy of a lifted air parcel is related to the specific reference density field along a vertical column passing through that parcel. Both concepts can be generalized for a vortical flow and to slantwise ascent of a lifted air parcel in such a flow. In all cases, the air parcel is assumed to have infinitely small dimensions. In this article, we explore the consequences of generalizing buoyancy and CAPE for buoyant regions of finite size that perturb the pressure field in their immediate environment. Quantitative calculations of effective buoyancy, defined as the sum of the conventional buoyancy and the static vertical perturbation pressure gradient force induced by it, are shown for buoyant regions of finite width. For a judicious choice of reference density, the effective buoyancy per unit mass is essentially a unique force, independent of the reference density, but its distribution depends on the horizontal scale of the buoyant region. A corresponding concept of "effective CAPE" is introduced and its relevance to deep convection in tropical cyclones is discussed. The study is conceived as a first step to understanding the decreasing ability of inner-core deep convection in tropical cyclones to ventilate the mass of air converging in the frictional boundary layer as the vortex matures and decays.

KEYWORDS

buoyancy, CAPE, deep convection, tropical convection, tropical cyclones

1 | INTRODUCTION

This article was motivated, in part, by attempts to understand the evolution of inner-core deep convection during the life cycle of a tropical cyclone. However, it soon became clear that the concepts are more widely applicable to convective systems in the Tropics and elsewhere. The terms "buoyancy" and "convective available potential energy"

(CAPE) are widely invoked concepts in relation to deep convection, in general, and to deep convection in the Tropics (including tropical cyclones) in particular. However, the limitations of these concepts are not always recognized or understood and can lead easily to arguments that are misguided or incomplete. A central problem is that air-parcel buoyancy as commonly defined is not a unique quantity because it depends on a reference density, which is usually chosen to characterize the density of the air parcel's environment. Nevertheless, CAPE, which is the vertical integral of the buoyancy, is considered to be a unique quantity, subject to the thermodynamic process assumed for the lifted air parcel and the parcel's height and thermodynamic state. Lucid articulations of the issues involved are provided by Doswell and Markowski (2004) and Houze (2014), whereas efforts to address these issues are described in articles by Davies-Jones (2003), Paluis and Garner (2006, section 4), and more recently by a number of other workers (Jeevanjee and Romps, 2015; 2016; Peters, 2016; Morrison, 2016; Tarshish *et al.*, 2018; McKim *et al.*, 2020).

With applications to deep convection in tropical weather systems and tropical cyclones in mind, in Sections 2 and 3 we review the definitions of buoyancy and CAPE and some of their limitations. Then, in Section 4, we review briefly the extension of these concepts to "air parcels" or buoyant regions of finite size following the insightful articulation of this extension by Houze (1993; 2014), which leads to the concepts of "effective buoyancy" (a term evidently first introduced by Davies-Jones (2003)) and "effective CAPE" as envisaged by Doswell and Markowski (2004). In Sections 5 and 6 we offer a range of calculations of effective buoyancy and effective CAPE relevant to the tropical atmosphere. In Section 7 we discuss some applications of the foregoing ideas to understanding tropical convection and tropical cyclones. In Appendix A we compare the Houze (1993) formulation with that of Davies-Jones (2003), highlighting some issues with the efforts of Peters (2016) to quantify "local buoyancy".

2 | BUOYANCY

In a non-rotating, inviscid fluid, the three-dimensional momentum equation is

$$\frac{\partial \mathbf{u}}{\partial t} + \mathbf{u} \cdot \nabla \mathbf{u} = -\frac{1}{\rho} \nabla p - g\mathbf{k}, \tag{1}$$

where $\mathbf{u}$ is the velocity vector, p is the pressure, ρ is the density, g is the acceleration due to gravity, and $\mathbf{k}$ is a unit vector in the local vertical direction. The left-hand side of the equation is just the vector acceleration of a fluid parcel

and the right-hand side is the force per unit mass acting on the parcel. Defining a reference density $\rho_o(z)$ and a reference pressure $p_o(z)$ that are in hydrostatic balance (i.e., $dp_o/dz = -g\rho_o$), Equation (1) may be written in terms of a "perturbation pressure" $p' = p - p_o(z)$ and a "buoyancy force" $b = -g(\rho - \rho_o)/\rho$, both per unit mass, to give

$$\frac{\partial \mathbf{u}}{\partial t} + \mathbf{u} \cdot \nabla \mathbf{u} = -\frac{1}{\rho} \nabla p' + b\mathbf{k}. \tag{2}$$

The vertical forces per unit mass on the right-hand sides of Equations (1) and (2) are the same; that is,

$$-\frac{1}{\rho}\frac{\partial p}{\partial z} - g = -\frac{1}{\rho}\frac{\partial p'}{\partial z} + b. \tag{3}$$

The numerator in the definition of b, that is, $-g(\rho - \rho_o)$, is sometimes referred to as the "Archimedean buoyancy force per unit volume" (e.g., Davies-Jones, 2003). The reference density can be arbitrary, but it is usually chosen to be density in the far environment or an areal average of the density over some domain. Although either side of Equation (3) is independent of the choice of reference density, p' and b are not. Thus, the buoyancy force and corresponding perturbation pressure gradient force are not uniquely defined: They depend on the choice of reference density.

In certain slowly spreading flows, such as buoyant plumes or buoyant jets, a scale analysis of the governing equations shows that the parcel buoyancy b dominates the perturbation pressure gradient $-(1/\rho)\partial p'/\partial z$, at least when the reference density is chosen to be that in the plume or jet environment (Morton *et al.*, 1956). However, if the reference density were chosen to be along the axis of the plume or jet, the buoyancy would be zero along the axis and negative elsewhere and the perturbation pressure gradient would be the dominant term. The same would be true for the updraught of a deep convective cloud, at least at altitudes where the updraught width is spreading only slowly with height. On the other hand, for some distance below the detrainment level where the updraught spreads out, a perturbation pressure gradient force, comparable in magnitude to the buoyancy force, is generally required to decelerate the updraught in the vertical and accelerate it horizontally (see Section 5).

By itself, the concept of buoyancy is limited because it is not the only vertical force and, depending in part on the choice of reference density in its definition, it may not be the dominant force in a particular situation. This feature was recognized in early modelling studies of convective clouds (see Holton, 1973 and references therein); we return to this feature in Section 5. A way to circumvent the non-uniqueness of buoyancy in the context of

moist convection was suggested by Davies-Jones (2003) and explored further by Peters (2016) (see Section 4).

In a rapidly rotating flow such as a tropical cyclone, the air parcel buoyancy will have a radial and a vertical component and the reference density may be generalized to be a function of both radius and height. In this case, one might wish to consider "local buoyancy" with respect to a background vortex that is in thermal wind balance (Smith *et al.*, 2005). The field of buoyancy associated with the background vortex would then be regarded as "system buoyancy".

3 | CAPE

Emanuel (1994) defines CAPE as the potential energy gained by an air parcel in rising from its current level z_i in a conditionally unstable atmosphere to its level of neutral buoyancy (LNB), whereas many others (e.g., Houze, 2014; Siebesma *et al.*, 2020) define it as the potential energy gained as the air parcel rises between its level of free convection (LFC) and its LNB. In practice, at least in the moist Tropics, the convective inhibition between z_i and the level of free convection is relatively small so that there is not much difference between the two definitions. In both cases, it is assumed that there is no mixing with environment air and that the lifted air parcel conserves either its pseudo-equivalent potential temperature (best for deep precipitating convection) or its reversible equivalent potential temperature (best for shallow non-precipitating convection).

Using the Emanuel (1994) definition, we may write

$$\text{CAPE} = \int_{z_i}^{\text{LNB}} b \, dz, \tag{4}$$

where z measures height and b is the buoyancy force per unit mass. The alternative definition, which we shall adopt here, may be written

$$\text{CAPE} = \int_{\text{LFC}}^{\text{LNB}} b \, dz. \tag{5}$$

In either definition, the reference density for calculating the buoyancy is always the profile of density along the vertical line that passes through the initial air parcel so that the buoyancy in Equations 4 and 5 is uniquely defined (e.g., Doswell and Markowski, 2004, p. 854). There are many caveats when using CAPE for estimating the energy of localized convective updraughts, one of which relates to the assumption that b is the sole vertical force acting on an air parcel, thereby neglecting the contribution from $(-1/\rho)\partial p'/\partial z$. The robustness of this assumption is explored in the following three sections. Other caveats regarding CAPE are reviewed in Section 6.1.

4 | BUOYANCY IN A FINITE HORIZONTAL DOMAIN

In section 7.2 of his book on cloud dynamics, Houze (1993; 2014) presents an elegant analysis of the way in which a region of buoyant air with finite size induces a static perturbation pressure field, p'_b, whose vertical gradient, $-(1/\rho)\partial p'_\text{b}/\partial z$ opposes the buoyancy force and whose magnitude increases with the horizontal scale of the buoyant region. The sum of these forces may be thought of as an effective buoyancy per unit mass:

$$b_\text{e} = -\frac{1}{\rho}\frac{\partial p'_\text{b}}{\partial z} + b. \tag{6}$$

Houze (2014) showed that when the buoyant region has infinitely small dimensions (i.e., the case of an air parcel), $-(1/\rho)\partial p'_\text{b}/\partial z$ is zero and $b_\text{e} = b$, while in the limit of infinite width, $-(1/\rho)\partial p'_\text{b}/\partial z$ exactly balances the buoyancy force and $b_\text{e} = 0$. In general, for a fluid in motion, there will be a dynamic contribution to the total perturbation pressure p', say p'_d, which is required to ensure the flow satisfies the mass continuity equation (see later). Houze's 2014 analysis is sketched in the next paragraph and provides the basis for a quantification of the relative contributions of $-(1/\rho)\partial p'_\text{b}/\partial z$ and b to b_e in a tropical context.

First, we make the "anelastic approximation" and replace the density by its horizontal average, $\rho_\text{o}(z)$, except where it appears in the buoyancy force. Multiplying Equation (2) by ρ_o and taking the three-dimensional divergence with the momentum advection term moved to the right-hand side gives

$$\frac{\partial}{\partial t}(\nabla \cdot \rho_\text{o}\mathbf{u}) = -\nabla^2 p' + \frac{\partial}{\partial z}(\rho_\text{o}b) - \nabla \cdot (\rho_\text{o}\mathbf{u} \cdot \nabla\mathbf{u}). \tag{7}$$

Using the anelastic form of the mass continuity equation, $\nabla \cdot (\rho_\text{o}\mathbf{u}) = 0$, Equation (7) may be written

$$\nabla^2 p' = \frac{\partial}{\partial z}(\rho_\text{o}b) - \nabla \cdot (\rho_\text{o}\mathbf{u} \cdot \nabla\mathbf{u})$$
$$= F_\text{b} + F_\text{d}, \tag{8}$$

where

$$F_\text{b} = \frac{\partial}{\partial z}(\rho_\text{o}b), \tag{9}$$

and

$$F_\text{d} = -\nabla \cdot (\rho_\text{o}\mathbf{u} \cdot \nabla\mathbf{u}). \tag{10}$$

Equation (8) is a Poisson-type, second-order, elliptic partial differential equation from which the perturbation pressure may be diagnosed, given the spatial distribution of F_b and F_d together with suitable boundary conditions on p'. The key step in the derivation of this equation is the use of the continuity equation. Physically, the equation constrains the pressure field in such a way that the total force (perturbation pressure gradient force and buoyancy force) produces a local flow acceleration at every point that is consistent with mass continuity together with suitable conditions on the flow boundary.

If the solution domain of Equation (8) is bounded by impermeable boundaries at the ground ($z = 0$) and at the tropopause ($z = H$) and if the forcing distributions are localized in the horizontal direction, Neumann boundary conditions, $\partial p'/\partial n = 0$, are appropriate boundary conditions to take, assuming that the side boundaries are sufficiently far from the forcing. Here, n refers to the direction normal to the particular boundary. These conditions would determine p' to within an arbitrary constant that could be taken to be zero at some point on one side boundary. From a dynamical perspective, it is only the perturbation pressure gradient that is of consequence. The condition that $\partial p'/\partial z = 0$ at $z = 0$ and $z = H$ is required for consistency with the vertical momentum equation when the vertical velocity is set to zero at these boundaries.

At this point it is convenient to partition the perturbation pressure into static and dynamic parts by writing $p' = p'_b + p'_d$. The solution of $\nabla^2 p'_b = F_b$ gives the static perturbation pressure distribution p'_b associated with the buoyancy distribution over a finite domain, whereas that of $\nabla^2 p'_d = F_d$ gives the perturbation pressure distribution p'_d associated with the instantaneous distribution of flow acceleration. Because the equation for p' is linear, there would be no loss of generality by choosing the same boundary conditions on p'_b and p'_d as on p', since these would ensure the correct conditions on p'.

Houze (2014) invoked an analogy with electrostatics to elucidate the qualitative behaviour of the solutions to $\nabla^2 p' = F_b + F_d$, but equally one could use the membrane analogy in which p' may be thought of as the equilibrium displacement of a stretched membrane in response to a steady force distribution $F_b + F_d$ applied normal to the membrane (cf. Wang and Smith, 2019).

A slightly different approach was suggested by Davies-Jones (2003) and discussed also by Doswell and Markowski (2004), but the outcome is the same. The Davies-Jones approach is to partition the static perturbation pressure p'_b into the sum of a non-hydrostatic part p'_{nh} and a hydrostatic part p'_h, where p'_h is chosen to satisfy the perturbation hydrostatic equation $(1/\rho_o)\partial p'_h/\partial z = b$. The details are sketched out in Appendix A, where the method is contrasted with the present approach.

In the next section we present some numerical solutions of Equation (8) in a bounded domain for specific buoyancy distributions that relate to the tropical atmosphere.

5 | QUANTIFICATION OF EFFECTIVE BUOYANCY

To elucidate the static perturbation pressure distribution p'_b induced by a finite region of buoyant air in a stably stratified environment, we examine two thought experiments. For simplicity, we assume a two-dimensional (slab symmetric) configuration in a domain that is 100 km wide, 16 km high, and with rigid horizontal boundaries at top and bottom, where $w = 0$.

In the first example, we consider the buoyancy distribution in a vertical column of finite width extending from an altitude of 2 km to 12 km, The background density within the domain $\rho_o(z)$ is taken to be a piecewise analytical approximation to the Dunion moist tropical sounding for the Atlantic hurricane season (Dunion, 2011), and the buoyancy in the column assumes a sinusoidal temperature perturbation over the column with a maximum amplitude of +3°C above the sounding temperature. The temperature perturbation is uniform across the column and zero at the upper and lower edges of the column. Details of the solution method and boundary conditions on perturbation pressure are given in Appendix B.

Figure 1 shows the fields of static perturbation pressure associated with column widths of 3 and 20 km. As anticipated by Houze (2014), the induced pressure perturbation increases as the width of the buoyant region increases. The buoyancy induces low perturbation pressure around the base of its region and high perturbation pressure around its top. This pattern would be consistent with the tendency for air to be drawn into the base of the buoyant region and to be forced upwards at the top, combined with a tendency for air to rise within the region itself (e.g., see Smith *et al.* (2005, figure 4 and related discussion), keeping in mind that a complete picture requires a consideration of the effects of F_d in Equation (8) as well). A similar demonstration of the scale effect on the perturbation pressure field was shown by Markowski and Richardson (2010, figure 3.1), and the same effect was noted by Trapp (2013, section 3.1.2). However, neither of these works showed the effective buoyancy force field.

Figure 2 shows vectors of static perturbation pressure gradient force per unit mass $-(1/\rho_o)(\partial p'_b/\partial x, \partial p'_b/\partial z)$ and the contours of the vertical component of this gradient corresponding to the calculations for the same columns shown in Figure 1. Supplementary to these panels, Figure 3 shows the vertical profiles of $-(1/\rho)\partial p'_b/\partial z$
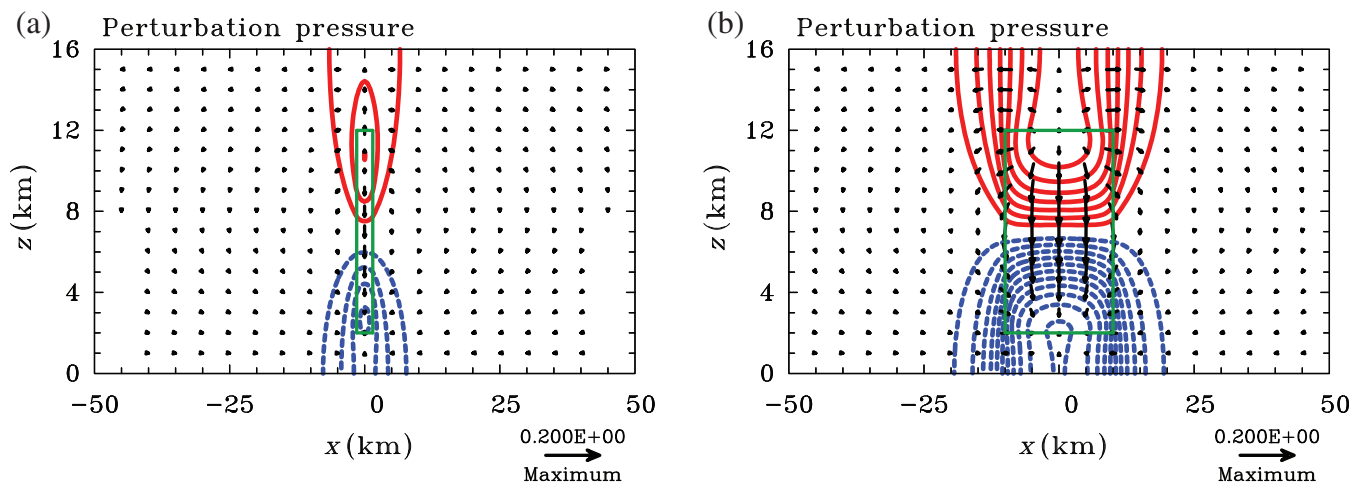
FIGURE 1 Static perturbation pressure field p_b' induced by a horizontally uniform sinusoidal temperature perturbation in the vertical to an analytical approximation to the Dunion Atlantic moist tropical sounding. This perturbation is applied in the region enclosed by the green rectangle centred at $x = 0$. It has a maximum amplitude of $+3°C$ and is zero at the upper and lower boundaries of the rectangle. Rectangle width: (a) 3 km; (b) 20 km. The contour interval for perturbation pressure is 20 Pa. Also shown are the vectors of perturbation pressure gradient force per unit mass. The reference scale for these vectors shown in the lower right is $0.2\,\mathrm{m \cdot s^{-2}}$ [Colour figure can be viewed at wileyonlinelibrary.com]
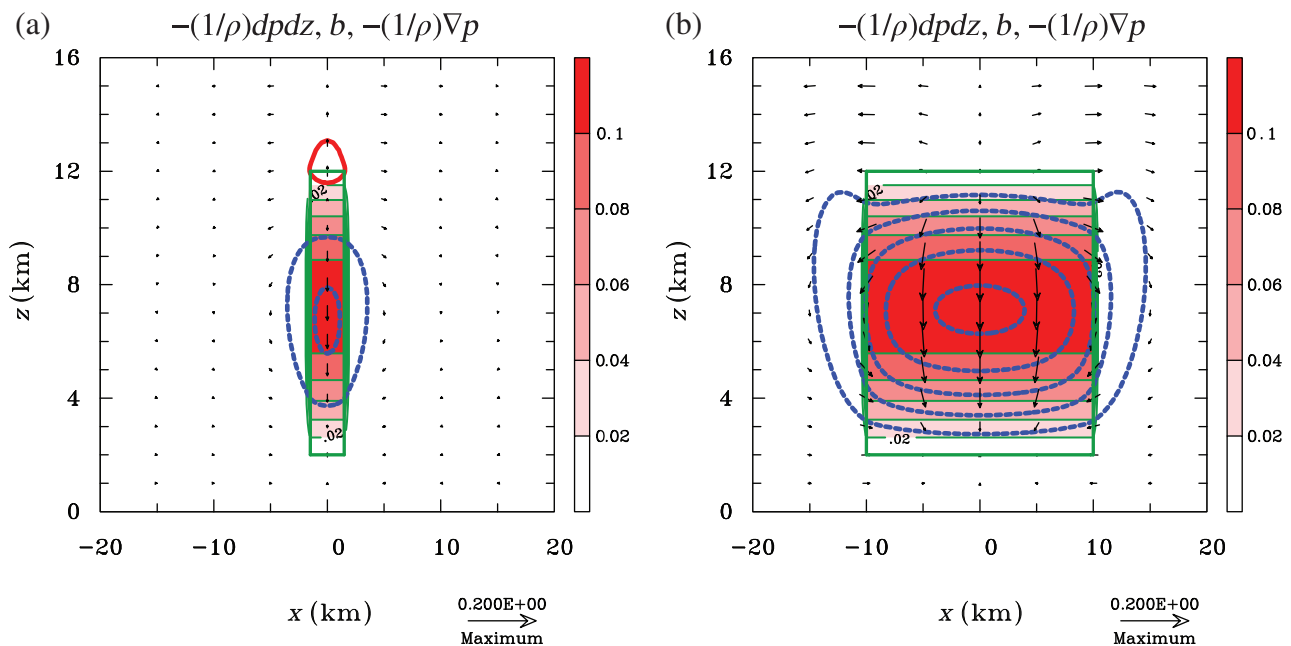

FIGURE 2 Buoyancy force b (green contours, colour shading) and static perturbation pressure gradient force per unit mass $-(1/\rho_o)(\partial p_b'/\partial x, \partial p_b'/\partial z)$ (arrows) corresponding to the calculations shown in Figure 1. The actual calculations were carried out on the same domain as Figure 1. Values on the colour bar in $\mathrm{m \cdot s^{-2}}$. The reference scale for the pressure gradient force vectors, $0.2\,\mathrm{m \cdot s^{-2}}$, is shown in the lower right. Red and blue contours show the vertical component of the perturbation pressure gradient force per unit mass. Contour interval $0.02\,\mathrm{m \cdot s^{-2}}$; solid red contours positive, dashed blue contours negative [Colour figure can be viewed at wileyonlinelibrary.com]

and b_e along the axis of the buoyancy column for these calculations and two additional columns with widths of 5 and 10 km. Figure 3b shows the vertical profile of b also, in essence the total static force for a column of infinitesimal width. Again, as anticipated by Houze (2014), as

the horizontal extent of the buoyant region increases, the contribution of $-(1/\rho)\partial p_b'/\partial z$ increases in magnitude and opposes the buoyancy force with the expectation that, as the horizontal scale becomes very large, the two forces almost cancel, leading to approximate hydrostatic balance.
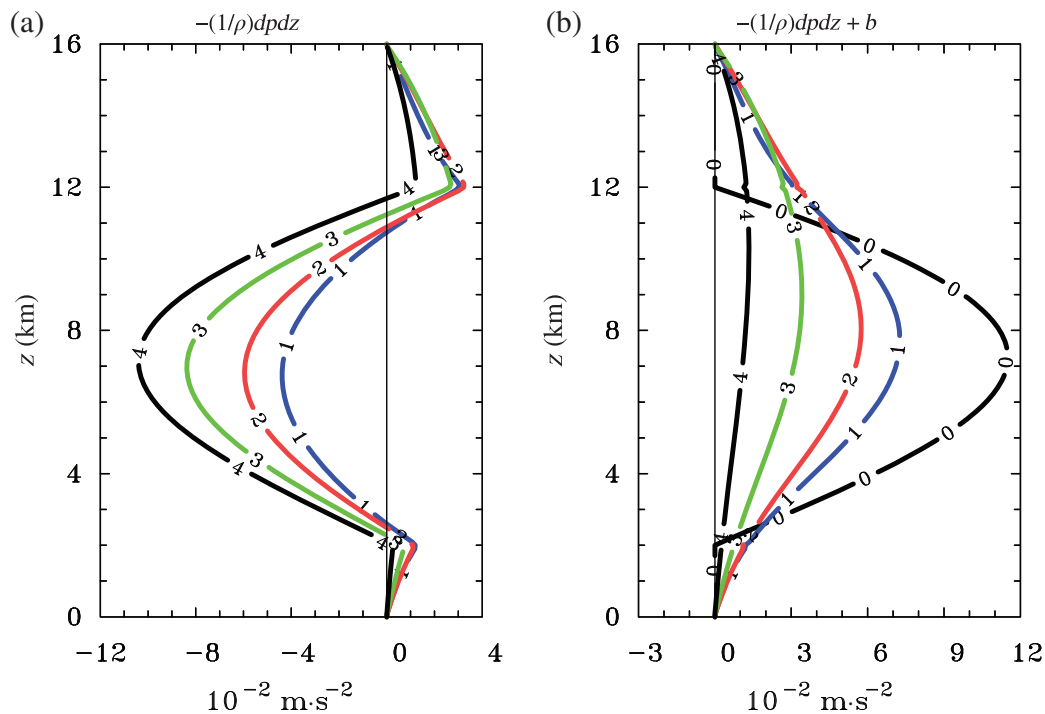
FIGURE 3 Vertical profiles of (a) static perturbation pressure gradient force per unit mass $-(1/\rho)\partial p_b'/\partial z$, and (b) the effective buoyancy per unit mass b_e, corresponding to the buoyancy distribution and sounding in Figure 1. Curves 1, 2, 3, and 4 refer to the forces along the axis of vertical columns of widths 3, 5, 10, and 20 km, respectively, and curve 0 refers to the buoyancy force alone corresponding to a column of infinitesimal width [Colour figure can be viewed at wileyonlinelibrary.com]

The perceptive reader will notice that the effective buoyancy force does not become negative below the top boundary, but the total force $-(1/\rho)\partial p'/\partial z + b$ must be negative since rising air parcels must decelerate before reaching this boundary. It follows that the deceleration effect must be contained in the solution of $\nabla^2 p_d' = F_d$, which gives the dynamical contribution to p'. To indicate that this is the case, we examine conditions along the vertical axis for simplicity. Along this axis, the lateral flow component is zero by symmetry and ignoring the decrease in density with height just below the top of the domain, F_d can be shown to be approximately equal to $-2\rho_o(\partial w/\partial z)^2$, which is negative definite (the derivation is sketched in Appendix C). According to the membrane analogy for solving the perturbation pressure equation (Wang and Smith, 2019), a region of negative F_d would imply one of positive total perturbation pressure p', as would be required to decelerate the vertical flow induced by the buoyancy force near the domain top.

In contrast to our definition of effective buoyancy per unit mass, Davies-Jones (2003) defines effective buoyancy per unit volume, which he shows to be completely independent of the reference density (see Appendix A). However, if one chooses a reference density judiciously so that the difference between $1/\rho$ and $1/\rho_o$ can be ignored, the effective buoyancy per unit mass (in essence the

second term in Emanuel (1994, equation (11.5.17)) would be essentially independent of reference density also. The questions then are what does the field of effective buoyancy look like and how does its distribution vary with the width of the region of buoyancy? Answers to these questions are provided by Figure 4, which shows contours of effective buoyancy b_e and vectors of the total force $(-(1/\rho_o)\partial p_b'/\partial x, b_e)$ corresponding to the four calculations referred to in Figure 3.

For each width of the buoyancy column, the effective buoyancy is positive both above and below the column from the surface to the top boundary and, in the narrower columns, the positive region is a little broader than the buoyancy column itself. Elsewhere, the effective buoyancy is negative with a narrow sheath of strong negative buoyancy along the side of the buoyancy column. As the width of the buoyancy column is increased, the maximum effective buoyancy moves away from the centre of the column, with the largest positive values along the inner edge of the column. At the same time, the effective buoyancy becomes smaller in the central region of the column. In essence, the largest values of effective buoyancy, both positive and negative, become concentrated along the sides of the buoyancy column. Note that even though the buoyancy itself is horizontally uniform across the buoyancy column, the effective buoyancy is not, a fact that will have consequences
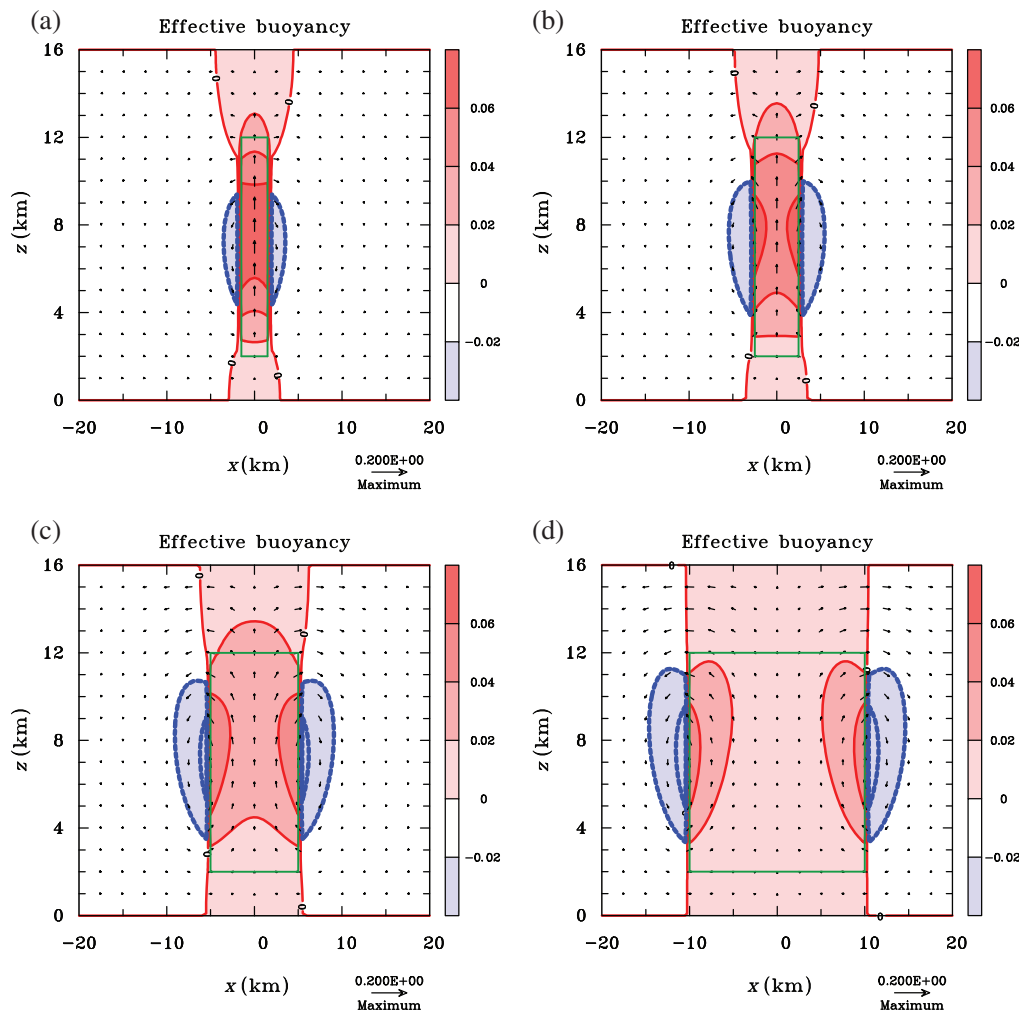
FIGURE 4 Effective buoyancy b_e (shaded) and vectors of the total static force $(-(1/\rho)\partial p'_b/\partial x, b_e)$ corresponding to the four calculations discussed in Section 5. Width of buoyancy region: (a) 3 km, (b) 5 km, (c) 10 km, (d) 20 km. Contour interval for effective buoyancy 0.02 m·s^{-2}; solid red contours positive, dashed blue contours negative. Values on the colour bar in m·s^{-2}. The reference scale for the pressure gradient force vectors, 0.2 m·s^{-2}, is shown in the lower right [Colour figure can be viewed at wileyonlinelibrary.com]

for calculating CAPE in a region of buoyancy of finite width. The concept of effective CAPE is explored in the next section.

The methodology for calculating effective buoyancy could be applied also to three-dimensional configurations of buoyancy, but this would involve solving the elliptic Poisson equation, Equation (8), in three dimensions instead of two.

6 | IMPLICATIONS FOR CAPE

The definition of CAPE given by Equation (4) or (5) considers only the buoyancy force acting on a lifted air parcel of infinitesimal size. Although this force is made unique by taking the reference density along a vertical through the lifted air parcel, it is strictly not the only force acting on the air parcel if the air parcel belongs to a region of buoyancy

with a finite size. As shown in the previous section, in this case, the perturbation pressure gradient force should be taken into account also.

It is clear from the substantial dependence of the total vertical force on the width of the buoyant region shown in Figure 3 that the conventional CAPE is likely to be a significant overestimate of potential energy achievable by an ascending air parcel, at least for an air parcel that rises along the axis of the buoyant column. By "effective CAPE" we mean the CAPE calculated with the total vertical force per unit mass acting on the air parcel. To demonstrate this fact, we calculate first the buoyancy distribution and CAPE in the usual way for an infinitesimally small air parcel lifted from an altitude of 100 m in the Dunion moist tropical sounding to its LNB. The positive buoyancy distribution between the LFC (about 900 m) and the LNB (about 13.8 km) is then used to calculate the total force on an air parcel within a buoyant column of finite width as
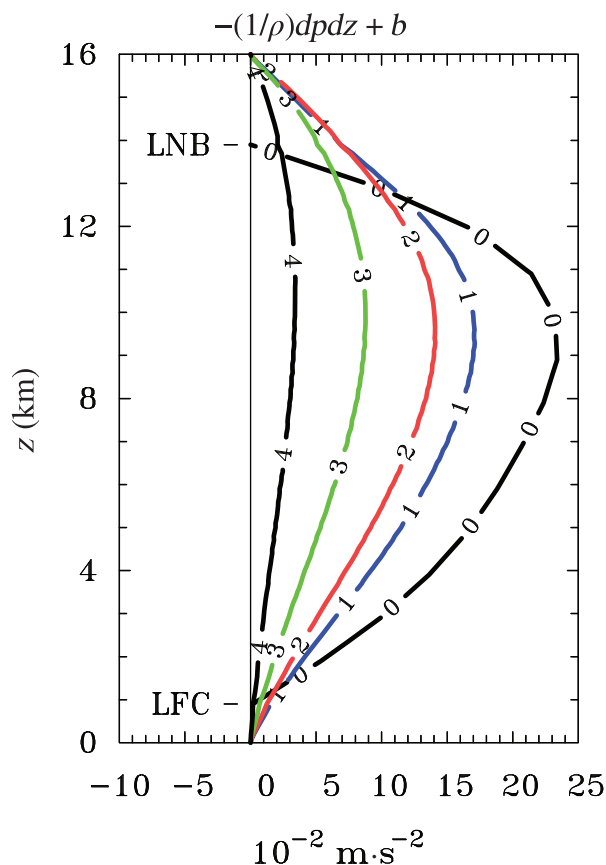
FIGURE 5 Vertical profiles of the effective buoyancy per unit mass of an air parcel lifted from a height of 100 m in the Dunion moist tropical sounding in regions of horizontally uniform buoyancy of different widths. Curves 1, 2, 3, and 4 refer to the specific forces along the axis of vertical columns of widths 3 km, 5 km, 10 km, and 20 km, respectively, and curve 0 refers to the pure buoyancy force for a column of zero width. The levels of free convection and neutral buoyancy for the lifted air parcel are denoted by LFC and LNB, respectively [Colour figure can be viewed at wileyonlinelibrary.com]

TABLE 1 Values of effective convective available potential energy (CAPE) for an infinitesimally small air parcel lifted along the axis of buoyant columns of finite width from a height of 100 m to the level of neutral buoyancy (LNB) in the Dunion moist tropical sounding. The calculations are based only on the "positive area"; that is, the vertical force between the level of free convection and LNB

Column width (km)	Effective CAPE (J·kg^{-1})
0	2,130
3	1,540
5	1,280
10	800
20	300

to the LNB is 100 m. The normal parcel CAPE, based on the buoyancy force alone, equivalent to a column width of 0 km, is approximately 2,130 J·kg^{-1}. However, as the column width increases to 20 km, the effective CAPE reduces to as little as 300 J·kg^{-1}.

It is worth noting that, like effective buoyancy, the effective CAPE in the foregoing calculations is a minimum along the axis of the buoyancy column and increases towards the edge of the column. Judging from Figure 4, this effect should be most pronounced for the larger column widths. Figure 6 highlights this feature for a lifted air parcel in the Dunion moist tropical sounding, showing the effective buoyancy and vectors of total force for the broadest buoyancy column with 20 km width. In the case of a buoyancy distribution without such an abrupt decline at its edge as here, it may be shown that the maximum effective CAPE occurs where the horizontal Laplacian of buoyancy is a maximum (Davies-Jones, 2003; see Equation (A4) in Appendix A).

It is worth noting here that Figures 4–6 complement some of the theoretical findings of Jeevanjee and Romps (2016) and Tarshish *et al.* (2018), based on axisymmetric buoyancy distributions centred at different heights above the surface. Jeevanjee and Romps' 2016 figures 1 and 3 are similar in spirit to our Figures 4 and 5. Likewise, Tarshish *et al.*'s 2018 figure 1 is similar to our Figure 4, except that they employ a spherically symmetric buoyancy distribution.

6.1 | Caveats on CAPE

Many researchers have cautioned against the indiscriminate use of parcel CAPE as a measure of convective instability and the vigour of convective updraughts. For example, Zipser (2003) draws attention to the importance
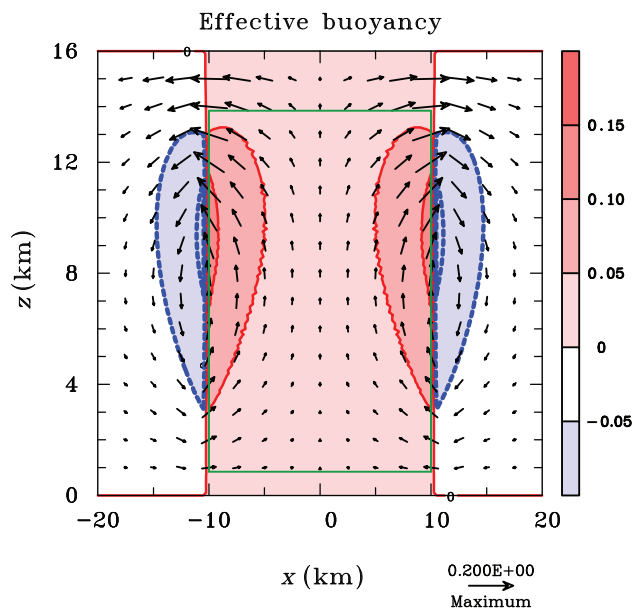
in Section 5. Where the buoyancy is negative, below the LFC and above the LNB, we set the buoyancy equal to zero for simplicity. We refer to the CAPE based on the effective buoyancy as the effective CAPE.

Figure 5 highlights conditions along the domain axis for four calculations corresponding to the same buoyancy columns in Figure 3, but with the buoyancy distribution calculated as described in this section. The figure shows the vertical profile of effective buoyancy b_e as in Figure 3b. In these cases also, the total vertical force is reduced significantly as the width of the buoyant column is increased on account of the increasing adverse perturbation pressure gradient force.

The effects of the decreasing total vertical force on the effective CAPE along the axis in these calculations is summarized in Table 1. In these calculations, the vertical interval for the integration of Equation (5) from the LFC

FIGURE 6 Effective buoyancy (shaded) and vectors of the total static force, $(-(1/\rho)\partial p'_b/\partial x, -(1/\rho)\partial p'_b/\partial z + b)$, for a lifted air parcel in the Dunion moist tropical sounding corresponding to the simulation with a buoyant region of 20 km width referred to in Figure 5. Contour interval for effective buoyancy 0.02 m·s^{-2}; solid red contours positive, dashed blue contours negative. Values on the colour bar in m·s^{-2}. The reference scale for the pressure gradient vectors, 0.2 m·s^{-2}, is shown in the lower right [Colour figure can be viewed at wileyonlinelibrary.com]

of turbulent mixing during the ascent of air in convective updraughts, noting that undilute ascent is rare and, if at all, is found only in severe convective storms in mid-latitudes. Citing observational studies by Lucas *et al.* (1994) and Wei *et al.* (1998), he argues that, in the case of oceanic deep convection in the Tropics, large dilution of convective updraughts by entrainment is the norm. Nevertheless, he argues that, despite large dilution, sub-cloud air can easily ascend within cumulonimbi to the tropopause if freezing of condensate is taken into account, supporting the results of an earlier study by Williams and Renno (1993) that, surprisingly, Zipser does not refer to.

Siebesma *et al.* (2020, section 2.3.3.2) point out the actual CAPE of a given atmospheric sounding "is not a number without ambiguity" and that "if it is to be used quantitatively, the particular use of the concept must be made precise". In general, CAPE is a function of the state of the air parcel lifted, the environment in which it is lifted, and the assumed thermodynamic process by which it is lifted.

Even if the concept of CAPE is made precise, comparison of CAPE values from different studies is often difficult because of differences in the way in which the initial thermodynamic state is determined, including the initial height of the lifted parcel and whether or not

its properties are based on some layer average. Observations by Renno and Williams (1995) found that convective updraughts have their roots at low levels in the boundary layer, and these authors recommend using lifted parcel heights between screen level and 100 m above the surface, a range similar to that suggested by Romps and Kuang (2011, section 1c). Notably, none of these authors discuss the potential limitations of CAPE estimates on account of the neglect of the vertical pressure gradient force investigated in the last three sections.

7 | SOME IMPLICATIONS FOR INTERPRETATIONS OF TROPICAL-CYCLONE CONVECTION

In a review article on tropical cyclone clouds, Houze (2010) writes:

> It is tempting to think of clouds in the inner regions of tropical cyclones as cumulonimbus that just happen to be located in a spinning vortex. However, this view is over simplified, as the clouds in a tropical cyclone are intrinsically connected with the dynamics of the cyclone itself.

A particular feature discussed in the review is the evolution of deep convection from upright buoyant cells that readily develop into mesoscale convective systems in the formation stage of the tropical cyclone, to slantwise structures with little parcel buoyancy that form the eyewall cloud complex as the mature stage is approached. It is certainly the experience of pilots flying hurricane reconnaissance missions that the most vigorous updraughts occur when the storm is in an early stage of development or rapidly intensifying. Nevertheless, Houze (2010) notes that, even in the mature stage, transient deep convective cells may develop in the eyewall complex that are more buoyant and more upright than the mean eyewall itself. Indeed, in a modelling study of Hurricane Bob (1991), Braun (2002) found that buoyant elements within the eyewall account for over 30% of the vertical mass flux in the eyewall. Other numerical simulations have shown the existence of two maxima in vertical velocity in the eyewall, one at low levels near where air exits the boundary layer and a second one in the upper troposphere, which is presumably a result of positive (effective) buoyancy; for example, see Smith *et al.* (2021, figure 4c,e).

Recent research has highlighted the fact that the net upward mass flux carried by deep convection in the inner core of a tropical cyclone should not be equated to the mass flux that converges in the frictional boundary layer,

as is done in many simple models. Rather, there is, in general, a mismatch between these quantities (Kilroy *et al.*, 2016; Wang and Smith, 2019; Smith *et al.*, 2021). If the vortex is still relatively weak, the boundary layer inflow will be weak and inner-core deep convection will be strong enough to draw air inwards above the boundary layer, opposing the tendency for the boundary layer to produce a shallow layer of outflow above it. The influx of the vertical component of absolute vorticity above the boundary layer will increase the azimuthal circulation, leading to vortex spin up. On the other hand, as the vortex strengthens, there may be periods in which the inner-core deep convection is no longer strong enough to ventilate all the air converging in the boundary layer. At such times, the fraction of air that cannot be ventilated will flow out above the boundary layer, leading to vortex spin down.

The foregoing studies indicate that, as the simulated tropical cyclone matures, the inner-core deep convection becomes increasingly less able to ventilate the mass converging in the boundary layer. It would be reasonable to surmise that the ability of deep convection to ventilate the mass of air converging in the boundary layer depends in some way on the collective buoyancy of updraughts, or more specifically on the effective buoyancy of the updraughts and the related CAPE.

Research aircraft surveys of the convective environment of pre-genesis disturbances during the PREDICT field campaign in 2010 (Montgomery *et al.*, 2012) corroborate the description by Houze (2010), showing that there were large values of pseudo-adiabatically calculated CAPE available to support vigorous deep convective systems in these disturbances (Smith and Montgomery, 2012). However, as summarized also by Houze (2010), in an azimuthally averaged view and to a first approximation, the eyewall convection in a mature tropical cyclone is close to a moist adiabat, whereupon there is only minimal buoyancy and hence minimal CAPE.

An early observational study by Bogner *et al.* (2000) provided evidence that, in hurricanes, there is a general increase in CAPE with radius from the centre, although this inference is based on sounding data below 500 mbar obtained by Omega dropsonde soundings. These data were complemented with composite reference soundings derived from radiosondes released from nearby land stations. Nevertheless, Bogner *et al.*'s finding is supported by a more comprehensive study by Molinari *et al.* (2012) using dropsondes released from an altitude closer to the tropopause, although in both of these studies the soundings were not obtained in the eyewall region itself.

Like Zipser (2003), Molinari *et al.* (2012) argued that CAPE values calculated with the normal assumptions, even assuming reversible ascent with no fusion, were unrealistically large, in that the maximum vertical velocities inferred from these values were much too large. They suggested that one needs to take entrainment into account, arguing that "entraining CAPE was consistent with the observed radial distribution of convective intensity … ". Though they acknowledged below their equation (1) the potential adverse effect of a negative perturbation pressure gradient force, they did not calculate this force, intimating they did not think it would be a dominant effect. However, from the data shown in their figure 3, the reduction in CAPE values to take account of entrainment are comparable to the reduction shown in our Table 1 as a result of the decrease in effective buoyancy with the width of the buoyant column. This reduction reflects the adverse vertical perturbation pressure gradient force for regions of convection with widths on the order of 20 km, which is comparable to the scale of convective rain bands observed in tropical cyclones (e.g., Houze, 2010; Bell *et al.*, 2012). This finding calls into question the conclusion that accounting for entrainment alone accounts for "the observed radial distribution of convective intensity". However, at this stage, it is premature to speculate on the relative roles of entrainment and the finite size of the convection on the calculation of CAPE because the vertical structure of the entrainment rate into clouds is poorly known.

Even though values of CAPE may be small in the eyewall of a tropical cyclone, it is clear that CAPE is not a very useful concept for assessing buoyancy in the eyewall. This is because the computed buoyancy of the lifted air parcel would be relative to a reference density[1] that lies within the eyewall, itself. As already noted herein, in the centre of such a moist environment, where the air is at, or close to, saturation over a considerable depth of the troposphere, one would not expect lifted air parcels to have much local buoyancy.

At least from an azimuthally averaged perspective, if the eyewall slope is not too large in the vertical, the relatively large width of the eyewall region would lead to a significant adverse perturbation pressure gradient force (see Section 5), and thereby to an even smaller effective buoyancy across much of the eyewall region. Of course, from a three-dimensional perspective, vertical shear in the azimuthal direction would be an additional complexity (e.g., Persing *et al.*, 2013). Strictly speaking, in either case, buoyancy and CAPE would need to be calculated along air parcel trajectories with an appropriate reference density that varies spatially (e.g., Braun, 2002). For example,

---

[1]In the presence of a rapidly rotating vortex one needs to decide whether or not to include or exclude the system buoyancy from the calculation; that is, the part of the buoyancy field that would be in thermal wind balance with the vortex in the definition of a reference density (Smith *et al.*, 2005).

in the azimuthally averaged perspective of a mature tropical cyclone, the eyewall may have an appreciable slope with height, so that the calculation of a slantwise CAPE would be more appropriate (e.g., Emanuel, 1994, chapter 12). Emanuel's definition is related in the vertical direction to the buoyancy and not to the effective buoyancy. The methodology for calculating effective buoyancy discussed here could be presumably generalized to slantwise CAPE, but it would need to consider the lateral (or radial) momentum equation as well.

The tropical-cyclone life cycle simulation described by Smith *et al.* (2021) indicates that, as the vortex matures, the eyewall expands and its mean radius increases. Despite this increase in area, it was shown that the eyewall becomes increasingly less capable of ventilating all the air that is being funnelled inwards in the frictional boundary layer. Again, it would be reasonable to surmise that the reduction of effective buoyancy that would accompany the expansion and areal growth of the eyewall would be an element of any explanation for the reduction of the areally averaged mass flux carried by the eyewall. An exploration of this likelihood is currently underway. This task will require, inter alia, an extension of the theory of buoyancy in a vortical flow by Smith *et al.* (2005) to one for effective buoyancy. It will require also an analysis of the dynamically induced pressure gradient field where the boundary layer terminates; that is, a solution of the $\nabla^2 p'_d = F_d$ part of Equation (8) formulated in cylindrical coordinates with appropriate consideration of centrifugal forces.[2]

8 | CONCLUSIONS

We have reviewed the widely used concepts of buoyancy and CAPE and their limitations in application to deep convection in tropical cyclones. As commonly defined, the buoyancy force of an air parcel is not unique because it depends on the arbitrary definition of a reference density field. However, one may define an "effective buoyancy" for buoyant regions of finite dimensions as the sum of the conventional buoyancy and the static vertical perturbation pressure-gradient force induced by it. For a judicious choice of reference density, the effective buoyancy per unit mass is essentially a unique force, independent of the reference density, but its distribution depends on the horizontal scale of the buoyant region.

We have presented calculations of effective buoyancy for idealized rectangular columns of horizontally uniform buoyancy of varying widths in a two-dimensional configuration where the background stability is based on a mean sounding for the tropical atmosphere. As the

buoyant region increases in width, appreciable values of effective buoyancy become concentrated near the sides of the buoyant region, while the effective buoyancy near the centre of the buoyancy column diminishes. The calculations motivate the introduction of a local "effective CAPE" based on the effective buoyancy. It is shown that, even when the buoyancy is horizontally uniform, the effective CAPE varies across the width of the buoyant region. As the buoyant column increases in width, the local effective CAPE at the centre of the column decreases compared with the actual CAPE.

The likely relevance of the calculations to understanding the evolution of buoyant deep convection in tropical cyclones was discussed. In this regard, the study was envisaged as a first step in understanding the decreasing ability of inner-core deep convection in tropical cyclones to ventilate the mass of air converging in the frictional boundary layer as the vortex matures and decays, as evidenced by recent studies.

AUTHOR CONTRIBUTIONS
R. K. Smith: writing – original draft; writing – review and editing. **M. T. Montgomery:** writing – original draft; writing – review and editing.

ORCID
R. K. Smith https://orcid.org/0000-0002-3668-1608
M. T. Montgomery https://orcid.org/0000-0001-5383-4648

REFERENCES
Bell, M.M., Montgomery, M.T. and Lee, W.C. (2012) An axisymmetric view of concentric eyewall evolution in Hurricane Rita (2005). *Journal of the Atmospheric Science*, 69, 2414–2432.

Bogner, P.B., Barnes, G.M. and Franklin, J.L. (2000) Conditional instability and shear for six hurricanes over the Atlantic Ocean. *Weather and Forecasting*, 15, 192–207.

Braun, S.A. (2002) A cloud resolving simulation of Hurricane Bob (1991): Storm structure and eyewall buoyancy. *Monthly Weather Review*, 130, 1573–1592.

Davies-Jones, R. (2003) An expression for effective buoyancy in surroundings with horizontal density gradients. *Journal of the Atmospheric Science*, 60, 2922–2925.

Doswell, C.A. and Markowski, P.M. (2004) Is buoyancy a relative quantity?. *Monthly Weather Review*, 132, 853–862.

[2]Coriolis forces should be weak in this inner region of the vortex.

Dunion, J.P. (2011) Rewriting the climatology of the tropical North Atlantic and Caribbean Sea atmosphere. *Journal of Climate*, 24, 893–908.

Emanuel, K.A. (1994) *Atmospheric convection*. New York, NY: Oxford University Press.

Holton, J.R. (1973) A one-dimensional cumulus model including pressure perturbations. *Monthly Weather Review*, 101, 201–205.

Houze, R.A. (1993) *Clouds dynamics*. San Diego, CA: Academic Press.

Houze, R.A. (2010) Clouds in tropical cyclones. *Monthly Weather Review*, 138, 293–343.

Houze, R.A. (2014) *Clouds dynamics* (2nd edn). London: Academic Press.

Jeevanjee, N. and Romps, D.M. (2015) Effective buoyancy, inertial pressure, and the mechanical generation of boundary layer mass flux by cold pools. *Journal of the Atmospheric Science*, 72, 3199–3213.

Jeevanjee, N. and Romps, D.M. (2016) Effective buoyancy at the surface and aloft. *Quarterly Journal of the Royal Meteorological Society*, 142, 811–820.

Kilroy, G., Smith, R.K. and Montgomery, M.T. (2016) Why do model tropical cyclones grow progressively in size and decay in intensity after reaching maturity?. *Journal of the Atmospheric Science*, 73, 487–503.

Lucas, C., Zipser, E.J. and LeMone, M.A. (1994) Vertical velocity in oceanic convection off tropical Australia. *Journal of the Atmospheric Science*, 51, 3183–3193.

Markowski, P. and Richardson, Y. (2010) *Mesoscale meteorology in low latitudes*. Oxford, UK: Wiley-Blackwell.

McKim, B., Jeevanjee, N. and Lecoanet, D. (2020) Buoyancy-driven entrainment in dry thermals. *Quarterly Journal of the Royal Meteorological Society*, 146, 415–425.

Molinari, J., Romps, D.M., Vollaro, D. and Nguyen, L. (2012) CAPE in tropical cyclones. *Journal of the Atmospheric Science*, 69, 2452–2462.

Montgomery, M.T., Davis, C., Dunkerton, T., Wang, Z., Velden, C., Torn, R., Majumdar, S., Zhang, F., Smith, R.K., Bosart, L., Bell, M.M., Haase, J.S., Heymsfield, A., Jensen, J., Campos, T. and Boothe, M.A. (2012) The Pre-depression Investigation of Cloud Systems in the Tropics (PREDICT) experiment: Scientific basis, new analysis tools, and some first results. *Bulletin of the American Meteorological Society*, 93, 153–172.

Morrison, H. (2016) Impacts of updraft size and dimensionality on the perturbation pressure and vertical velocity in cumulus convection. Part I: Simple, generalized analytic solutions. *Journal of the Atmospheric Science*, 73, 1441–1454.

Morton, B.R., Taylor, G.I. and Turner, J.S. (1956) Turbulent gravitational convection from maintained and instantaneous sources. *Proceedings of the Royal Society A*, 234, 1–23.

Paluis, O. and Garner, S. (2006) Sensitivity of radiative–convective equilibrium simulations to horizontal resolution. *Journal of the Atmospheric Science*, 63, 1910–1923.

Persing, J., Montgomery, M.T., McWilliams, J. and Smith, R.K. (2013) Asymmetric and axisymmetric dynamics of tropical cyclones. *Atmospheric Chemistry and Physics*, 13, 12299–12341.

Peters, J.M. (2016) The impact of effective buoyancy and dynamic pressure forcing on vertical velocities within two-dimensional updrafts. *Journal of the Atmospheric Science*, 73, 4531–4551.

Renno, N.O. and Williams, E.R. (1995) Quasi-Lagrangian measurements in convective boundary layer plumes and their implications for the calculation of CAPE. *Monthly Weather Review*, 123, 2733–2742.

Romps, D.M. and Kuang, Z. (2011) A transilient matrix for moist convection. *Journal of the Atmospheric Science*, 68, 2009–2025.

Siebesma, A.P., Bony, S., Jakob, C. and Stevens, B. (2020) *Clouds and climate: Climate science's greatest challenge*. Cambridge, UK: Cambridge University Press.

Smith, R.K., Kilroy, G. and Montgomery, M.T. (2021) Tropical cyclone life cycle in a three-dimensional numerical simulation. *Quarterly Journal of the Royal Meteorological Society*, 147, 3373–3393.

Smith, R.K. and Montgomery, M.T. (2012) Observations of the convective environment in developing and non-developing tropical disturbances. *Quarterly Journal of the Royal Meteorological Society*, 138, 1721–1739.

Smith, R.K., Montgomery, M.T. and Zhu, H. (2005) Buoyancy in tropical cyclones and other rapidly rotating vortices. *Dynamics of Atmospheres and Oceans*, 40, 189–208.

Tarshish, N., Jeevanjee, N. and Lecoanet, D. (2018) Buoyant motion of a turbulent thermal. *Journal of the Atmospheric Science*, 75, 3233–3244.

Trapp, R.J. (2013) *Mesoscale convective processes in the atmosphere*. Cambridge, UK: Cambridge University Press.

Wang, S. and Smith, R.K. (2019) Consequences of regularizing the Sawyer–Eliassen equation in balance models for tropical cyclone behaviour. *Quarterly Journal of the Royal Meteorological Society*, 145, 3766–3779.

Wei, D., Blyth, A.M. and Raymond, D.J. (1998) Buoyancy of convective clouds in TOGA COARE. *Journal of the Atmospheric Science*, 55, 3381–3391.

Williams, E.R. and Renno, N.O. (1993) An analysis of the conditional instability of the tropical atmosphere. *Monthly Weather Review*, 121, 21–36.

Zipser, E.J. (2003). Some views on "hot towers" after 50 years of tropical field programs and two years of TRMM data. In: W.-K. Tao and R. Adler (Eds.), *Cloud systems, hurricanes, and the Tropical Rainfall Measuring Mission (TRMM): A tribute to Dr. Joanne Simpson* (pp. 49–58). Boston, MA: American Meteorological Society.

APPENDIX A. EFFECTIVE BUOYANCY PER UNIT MASS

As noted in Section 4, Davies-Jones (2003) partitions the static perturbation pressure p'_b into the sum of a non-hydrostatic part p'_{nh} and a hydrostatic part p'_h,

where p'_h is chosen to satisfy the perturbation hydrostatic equation

$$\frac{1}{\rho_o} \frac{\partial p'_h}{\partial z} = b. \tag{A1}$$

Then, the vertical component of the momentum equation has the form

$$\frac{Dw}{Dt} = \frac{1}{\rho_o} \left(\frac{\partial p'_d}{\partial z} + \frac{\partial p'_{nh}}{\partial z} \right), \tag{A2}$$

where $Dw/Dt = \partial w/\partial t + \mathbf{u} \cdot \nabla w$ is the vertical acceleration. Note that the buoyancy b and vertical gradient of static perturbation pressure p'_b per unit mass have combined to give $(1/\rho_o)\partial p'_{nh}/\partial z$.

After a little algebra, the equation corresponding to Equation (8) becomes one for p_{nh}; that is,

$$\nabla^2 p'_{nh} = F_h + F_d, \tag{A3}$$

where $F_h = -\nabla_h^2 p'_h$ and F_d is as in Section 4. Davies-Jones (2003) takes $-\partial/\partial z$ of Equation (A3) and uses Equation (A1) to obtain

$$\nabla^2 \left(-\frac{\partial p'_{nh}}{\partial z} \right) = -g\rho_o \nabla_h^2 b. \tag{A4}$$

He notes also that if $w = 0$ at $z = 0$, the right-hand side of Equation (A2) must be zero at $z = 0$. Further, he goes on to assume that the two pressure gradient terms on the right-hand side of Equation (A2) are separately zero at $z = 0$, whereupon Equation (A4) may be solved, in principle, subject to Dirichlet (*sic*) boundary conditions on $\partial p'_{nh}/\partial n$ (i.e., $\partial p'_{nh}/\partial n = 0$ along the domain boundary as in Section 4).

Davies-Jones (2003) defines $-\partial p'_{nh}/\partial z$ as the "effective buoyancy per unit volume" and notes that, because the term $g\rho_o \nabla_h^2 b$ on the right-hand side of Equation (A4) is independent of the reference density, so must this effective buoyancy. Nevertheless, effective buoyancy per unit mass $-(1/\rho_o)\partial p'_{nh}/\partial z$ does depend on the choice of reference density. Davies-Jones (2003) obtained a formal solution of Equation (A4) in terms of a Green's function in the half space $z > 0$, but did not show specific solutions.

More recently, Peters (2016) attempted to solve the two-dimensional (x, z) form of Equation (A4) for a localized region of buoyant air with width δx and depth between the LFC to the LNB. However, this solution is limited by the fact that boundary conditions

$\partial p'_{nh}/\partial z|_{\text{LFC}} = 0$, $\partial p'_{nh}/\partial z|_{\text{LNB}} = 0$ and $\partial p'_{nh}/\partial z|_{\pm\delta x} = 0$ are applied on the boundaries of the buoyant region rather than along the boundaries of the whole domain that encompasses the buoyant region and its environment.

APPENDIX B. SOLUTION OF EQUATION (8)

The Poisson-type second-order partial differential equation in Equation (8) is solved explicitly for the perturbation pressure p' on a rectangular grid using the solver helmholtz_ffacr.f90 (available from the first author). The domain is 100 km wide and 16 km high with a grid spacing of 500 m in the horizontal direction and 100 m in the vertical, equivalent to 201×161 grid points. Neumann conditions are imposed on p' along each boundary (see Section 4) and the solution is made unique by the requirement that $p' = 0$ at the lower left corner of the domain.

APPENDIX C. FORCING OF p' BY F_d IN EQUATION (8) ON THE UPPER DOMAIN AXIS

Taking $\mathbf{u} = (u, w)$, $F_d = -\nabla \cdot (\rho_o \mathbf{u} \cdot \nabla u, \rho_o \mathbf{u} \cdot \nabla w)$, or

$$F_d = -\frac{\partial}{\partial x} \left(\rho_o u \frac{\partial u}{\partial x} + \rho_o w \frac{\partial u}{\partial z} \right)$$
$$- \frac{\partial}{\partial z} \left(\rho_o u \frac{\partial w}{\partial x} + \rho_o w \frac{\partial w}{\partial z} \right) \tag{C1}$$

while mass continuity, Equation (3), gives

$$\frac{\partial u}{\partial x} = -\frac{1}{\rho_o} \frac{\partial}{\partial z}(\rho_o w). \tag{C2}$$

Then, Equation (C1) becomes

$$F_d = -\frac{1}{\rho_o} \left[\frac{\partial}{\partial z}(\rho_o w) \right]^2 + u\frac{\partial}{\partial x} \left[\frac{\partial}{\partial z}(\rho_o w) \right]$$
$$- \rho_o \frac{\partial w}{\partial x} \frac{\partial u}{\partial z} + \rho_o w \frac{\partial}{\partial z} \left[\frac{1}{\rho_o} \frac{\partial}{\partial z}(\rho_o w) \right]$$
$$- \frac{\partial}{\partial z} \left(\rho_o u \frac{\partial w}{\partial x} + \rho_o w \frac{\partial w}{\partial z} \right). \tag{C3}$$

Along the axis $x = 0$, $u = 0$ and $\partial w/\partial x = 0$ by symmetry, whereupon

$$F_d = -\frac{1}{\rho_o} \left[\frac{\partial}{\partial z}(\rho_o w) \right]^2 - \frac{\partial}{\partial z} \left(\rho_o w \frac{\partial w}{\partial z} \right). \tag{C4}$$

Assuming that near the domain top, the Boussinesq approximation is valid (i.e., ρ_o is approximately constant), it follows that

$$F_d \approx -2\rho_o \left(\frac{\partial w}{\partial z} \right)^2, \tag{C5}$$

which is negative definite and, according to the membrane analogy (see Section 4), would lead to a positive perturbation pressure near the top of the domain, as expected.